 ISSN 0267-8179. DOI: 10.1002/jqs.3027

JQS Journal of Quaternary Science QRA Quaternary Research Association

Holocene temperature trends in the extratropical Northern Hemisphere based on inter-model comparisons

YURUI ZHANG,[1,2]* HANS RENSSEN,[2,3] HEIKKI SEPPÄ[1] and PAUL J. VALDES[4]
[1]Departmentof Geosciences and Geography, University of Helsinki, Helsinki, Finland
[2]Department of Earth Sciences, VU University Amsterdam, Amsterdam, The Netherlands
[3]Department of Natural Sciences and Environmental Health, University College of Southeast Norway, Bø, Norway
[4]School of Geographical Sciences, University of Bristol, Bristol, UK

Received 23 May 2017; Revised 29 November 2017; Accepted 27 January 2018

ABSTRACT: Large uncertainties exist in Holocene climate estimates, especially for the early Holocene when large-scale reorganization occurred in the climate system. To improve our understanding of these uncertainties, we compare four Holocene simulations performed with the LOVECLIM, CCSM3, HadCM3 and FAMOUS climate models. The simulations are generally consistent for the large-scale Northern Hemisphere extratropics, while the multi-simulation consistencies are heterogeneous on the sub-continental scale. Consistently simulated temperature trends are found in Greenland, northern Canada, north-eastern and north-western Europe, and central-west Siberia. These Holocene temperatures show a pattern of an early Holocene warming, mid-Holocene warmth and gradual decrease towards the pre-industrial in winter, and the extent of early Holocene warming varies spatially, with 9 °C warming in northern Canada compared with 3 °C warming in central-west Siberia. In contrast, mismatched temperatures are detected: in Alaska, the warm early Holocene winter in LOVECLIM primarily results from strongly enhanced southerly winds induced by the ice sheets; in eastern Siberia, the intense early-Holocene summer warmth anomaly in CCSM3 is caused by large negative albedo anomalies due to overestimated snow cover at 0 ka; in the Arctic, cool winter conditons in FAMOUS can be attributed to extensive sea ice coverage probably due to simplified sea ice representations. Thus, the Holocene temperature trends in these regions remain inconclusive. Copyright © 2018 John Wiley & Sons, Ltd.

KEYWORDS: climate sensitivity; extratropical Northern Hemisphere; Holocene temperature; ice sheets and meltwater; inter-model comparisons.

Introduction

The Holocene is an important period for investigating climate variability and improving our understanding of the climate system due to detectable changes in climate variables and an abundance of available proxy records. The early Holocene (11.5–7 ka) was a transitional period, accompanied by reorganizations in several components of the climate system (*e.g.* CAPE project members, 2001; Dyke *et al.*, 2003; Shakun *et al.*, 2012). Investigating this transient period can increase our understanding of climate system variabilities, and provide further information on climate history. Climate modelling is a useful tool to investigate climate change, and thus has the potential to improve our understanding of the indeterminate early Holocene climate, especially based on transient simulations. Recent model simulations have either included or specifically focused on this critical period to investigate climate responses to dynamic climate forcings (He, 2011; Zhang *et al.*, 2016). However, uncertainties related to the melting of ice sheets adds a challenge in accurately simulating the climate of this period. The ice-sheet-related uncertainty during the early Holocene has been tested by Zhang *et al.* (2016), who investigated two different freshwater scenarios in model simulations to identify a more reasonable scenarios of the early-Holocene climate and the timing of the Holocene Thermal Maximum.

Uncertainties in the early Holocene simulations are not only the result of ambiguity in climate forcings, but also of model-dependent variations. The performance of models and their sensitivities to given forcings are primarily determined by the physical representations of various climate processes in the models. For instance, climate sensitivity to radiative forcings (CSr) usually refers to the change in the global annual mean surface air temperature (in °C) experienced by the climate system after it has attained a new equilibrium in response to a doubling of atmospheric CO_2 concentration (Knutti and Hegerl, 2008). Estimates of CSr vary from 2.1 to 4.7 °C among the models in the Coupled Model Intercomparison Project (CMIP5), due to various feedbacks involved in the models (Randall *et al.*, 2007; Flato *et al.*, 2013). In addition, CSr is greater for cold than for warm climates, and the sensitivities to changes in climate conditions differ among individual studies owing to non-uniform representations of cryospheric processes or dynamic ocean feedback processes (Boer and Yu, 2003; Randall *et al.*, 2007; Kutzbach *et al.*, 2013). Variations among models in the estimates of key climate process or parameters, such as the climate-state-dependent CSr, add extra difficulties to simulating the early Holocene climate.

Multi-model comparison provides an option to validate the reliability of model performances and hence to increase the confidence in simulations. The reliability of and confidence in simulations increases if similar features are observed in other independent model results; conversely, further investigations are required when multi-model simulations differ. The Paleoclimate Modeling Inter-Comparison Project (PMIP) has performed a wide range of inter-model comparisons, covering a series of periods, such as the Last Glacial Maximum (LGM, 21 ka), the Last Interglacial (130–115 ka)

*Correspondence to: Yurui Zhang, [1]Department of Geosciences and Geography, as above.
Email: yurui.zhang@helsinki.fi

and the mid-Holocene (6 ka) (*e.g.* Harrison *et al.*, 1998; Braconnot *et al.*, 2000; Lunt *et al.*, 2013). However, the PMIP comparisons for the Holocene primarily focus on the mid-Holocene with snapshot experiments, and previous transient inter-model comparisons have only been conducted for periods shorter than the whole Holocene period, such as 8–2 ka and the last millennium (*e.g.* Bakker *et al.*, 2014) to avoid the uncertainty related to impact of ice sheets on the climate. Therefore, the question of how similar or different the model simulations are during the early Holocene remains unknown, and inter-model comparisons spanning the entire Holocene are of great value.

Here, we evaluate the robustness of four different simulations covering the whole Holocene in detail by conducting inter-model comparisons and analysing their uncertainties. These four models are LOVECLIM (Zhang *et al.*, 2016), CCSM3 (He, 2011), HadCM3 (Singarayer and Valdes, 2010), and FAMOUS (this study), and they differ in multiple critical aspects, as summarized in Table 1. Our goal is to analyse how the climate responds to dominant forcings in these different models and to evaluate how robust these responses are based on comparisons of multiple Holocene transient simulations. In particular, our comparisons aim to: (i) identify the agreements and divergences among these Holocene simulations, (ii) detect which aspects of the climate system in simulations cause these multi-model variations, and (iii) further examine the potential origin of these inconsistencies, such as different parameterizations and biases in the models. A detailed data–model comparison is, however, beyond the scope of the present study, and will be the topic of a future publication.

Models and simulations

Models and prescribed climate forcings

The climate models used in this study, LOVECLM, FAMOUS, CCSM3 and HadCM3, have various resolutions and complexities. Key information regarding these models is summarized in Table S1 and more detailed information can be found in the Supporting Information. We included major climatic forcings in terms of insolation variation on orbital scale (ORB), greenhouse gases (GHG) (Fig. S1) in the atmosphere and decaying ice sheets [ice-sheet configuration (ISC) and associated freshwater fluxes (FWF)]. Other forcings, such as the solar constant and aerosol levels, were kept fixed at pre-industrial values in all simulations. More detailed information on the climate forcings is given in the Supporting Information.

Set-up of simulations

The LOVECLIM simulation is an 115-ka-long transient run that was initialized from an equilibrium experiment (more details are provided by Zhang *et al.*, 2016). The simulation was forced by the annually varied ORB and GHG throughout the entire period. In addition, the prescribed ISC was included with a time step of 250 years until 6.8 ka when the ice sheet eventually disappeared, and associated FWF was also applied with a stepwise time series (Fig. 1). The CCSM3 simulation was taken from the TraCE-21ka project, which is a 21-ka-long simulation forced by transient ORB, GHG, ISC and FWF. ISCs were modified every 500 years based on the ICE-5G reconstructions. Freshwater was discharged with irregular time steps until 6 ka (He, 2011). The FAMOUS simulation is also the Holocene part of a 21-ka simulation that was forced by the transient GHG and ORB forcings, with prescribed ISC and freshwater from the melting of ice sheets. The HadCM3 results were derived from two sets of snapshot experiments at 1-ka intervals; and the GHG, ORB and ice sheet forcings were updated in each snapshot. The main reason for including these experiments is that the high spatial resolution of the HadCM3 model allows a direct test of the impact of resolution and complexity, although differences between transient and equilibrium adds complexity to comparisons. The differences between these two sets of experiments are the ice sheet configurations, which were based on ICE-I5G and ICE-I6G, respectively, and they were accordingly named HadCM3-I5G and HadCM3-I6G. Given the similarity between HadCM3-I5G and HadCM3-I6G, they are generally considered as an HadCM3 simulation unless specifically indicated. Each of these snapshot experiments was initialized from a spun-up pre-industrial simulation (Singarayer and Valdes, 2010) and was run for at least 300 years with fixed GHG and ORB forcings, of which the last 30-year average was taken as representative of the climate during the corresponding time window. The main information on these simulations is summarized in Table 1.

The model name is also used as an indicator of the corresponding simulation to reduce redundancies. Temperatures presented are simulated surface temperatures, and are shown as the deviations from 0 ka (the pre-industrial). To obtain the overall temperature trend throughout the Holocene, the ensemble mean was calculated by averaging all transient simulations. This implies that the HadCM3 results were not included in the ensemble and are separately shown in figures.

Table 1. Main features of the set-up of the simulations investigated.

		Simulation			
		LOVECLIM	CCSM3	HadCM3	FAMOUS
Prescribed forcing and reference	ORB	Berger (1978)	Berger (1978)	Berger and Loutre (1991)	Berger and Loutre (1991)
	GHG	Loulergue *et al.* (2008), Schilt *et al.* (2010)	Joos and Spahni (2008)	Spahni *et al.* (2005), Loulergue *et al.* (2008)	Spahni *et al.* (2005), Loulergue *et al.* (2008)
	Icesheet*	Icesheet, FWF	Icesheet, FWF	Icesheet	Icesheet, FWF
Initial condition		Eq_11.5 ka (1.2 kyr)	Tran_21 kyr	Pre-industrial snapshot	Tran_21 kyr
Length_exp		11.5 kyr	21 kyr	Multiple snapshots	21 kyr
Reference for simulation		Zhang *et al.* (2016)	He (2011)	Singarayer and Valdes (2010)	This study

*Includes the Laurentide Ice Sheet, Fennoscandia Ice Sheet and Greenland Ice Sheet.

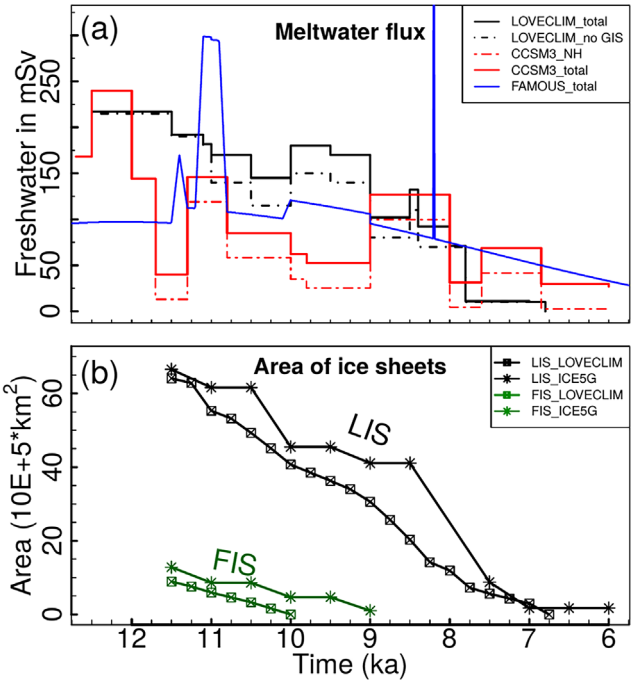

Figure 1. Ice-sheet-related forcings during the early Holocene. (a) Prescribed freshwater flux (in mSv) into oceans, and (b) the area of ice sheets (km^2) in the simulations.

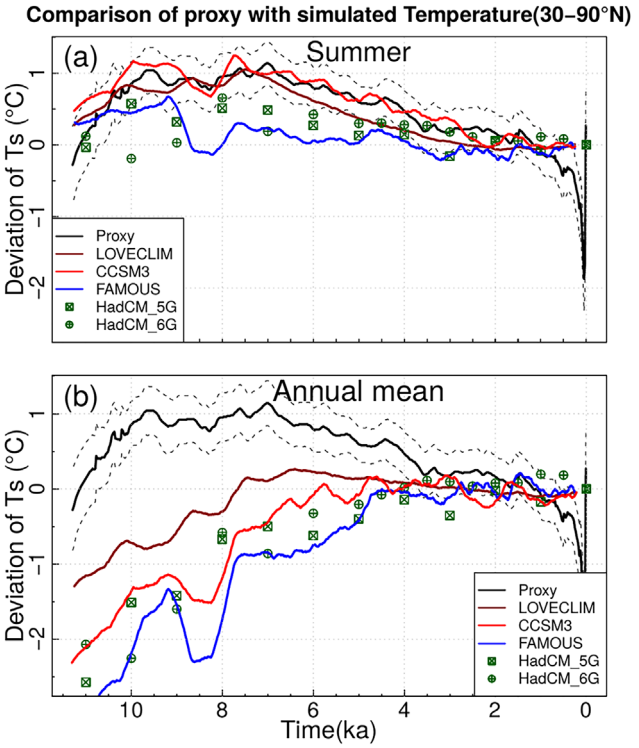

Figure 2. Comparison of stacked proxy reconstruction with simulated summer (a) and annual mean temperature (b) in the Northern Hemisphere extratropics (over 30–90°N), shown as a deviation from 0 ka. The stacked temperature reconstruction with 1σ uncertainty (dashed lines) is based on Marcott *et al.* (2013). The proxy curve is the same in (a) and (b), although the authors interpreted it as annual mean.

Results

Simulated temperature in the Northern Hemisphere extratropics

Although HadCM3 and FAMOUS show a slightly cooler climate until 5 ka than CCSM3 and LOVECLIM, the simulated summer temperature trends in the Northern Hemisphere extratropics (30–90°N) are generally consistent across the models (Fig. 2a). They reveal an early Holocene warming, a maximum temperature at 10–7 ka and a cooling towards 0 ka. In summer, the magnitudes of early Holocene anomalies in these models roughly correlate to their climate sensitivities, as high sensitivity implies a large climate response to given forcings (Fig. 2b; Table S1). The simulated annual mean temperature shows a gradual warming of about 2 °C by 4 ka, after which the temperature stays at the 0 ka value (Fig. 2b). There is a 1 °C spread in simulated annual mean temperature before 5 ka, with the coolest climate in FAMOUS and warmest in LOVECLIM. An abrupt cooling at ~8.5 ka is found in both the CCSM3 and the FAMOUS simulations.

To evaluate the reliability of the simulations approximately, the simulated results are briefly compared with proxy data. The proxy data are stacked temperatures based on proxy records from 30° to 90°N (Marcott *et al.*, 2013). This model data comparison reveals an overall agreement, despite a slightly stronger early Holocene warming until 9.5 ka suggested by the proxy data. In particular, the simulated summer temperatures show better agreement with proxy data than annual mean temperatures, which is consistent with the suggestion of potential seasonal biases in the biological proxy data (Lohmann *et al.*, 2013; Liu *et al.*, 2014).

Strong spatial patterns of simulated temperatures are found when zoomed in to the regional scale. To further illustrate the regional climate response to relevant forcings, two periods, 11.5 and 6 ka, were selected as specific time windows. These two time windows either represent the period when the ice sheets played important roles, or serve as a benchmarking epoch (*e.g.* in PMIPs). Simulated temperatures generally show negative anomalies at 11.5 ka, with a magnitude of −1 to −5 °C in annual mean temperatures, except in Beringia where positive temperature anomalies are found in LOVECLIM and CCSM3 (Fig. 3). The temperatures at 6 ka show a latitudinal pattern. At mid-latitudes, simulations suggest similar or slightly lower temperature than at 0 ka. At high latitudes, annual mean temperatures show model dependencies: 1–3 °C higher temperatures in CCSM3 and LOVECLIM contrast with a similar or −0.5 °C cooler climate in FAMOUS and HadCM3. These results seem agree with PMIP2-related studies for the mid-Holocene climate. For instance, this spatial pattern of simulated temperature matches the results of Brewer *et al.* (2007), who analysed PMIP2 simulations and revealed a spatial pattern of cooler south and warm north over Europe. The model dependencies might imply model biases, which has been demonstrated by Jiang *et al.* (2012) who compared the PMIP2 simulations with the proxy-based reconstruction and found that climate models under-estimated the mid-Holocene temperature in China by more than 3 °C in summer. In addition, the differences between the present and previous studies can be partly explained by the snapshot or transient simulations. Another significant feature of climate during the early Holocene is that the multi-model consistencies are regionally heterogeneous and generally larger in winter than in summer. Target regions were further selected according to the spatial pattern of climate response to dominant forcings (Fig. S2), and the Holocene temperature trends over these regions were analysed. Based on their consistencies, these selected regions were divided into two groups, representing consistent and inconsistent areas. The first group is formed by Greenland, northern Canada, north-eastern Europe, north-western Europe and central-west Siberia, as all models give similar early Holocene temperature trends.

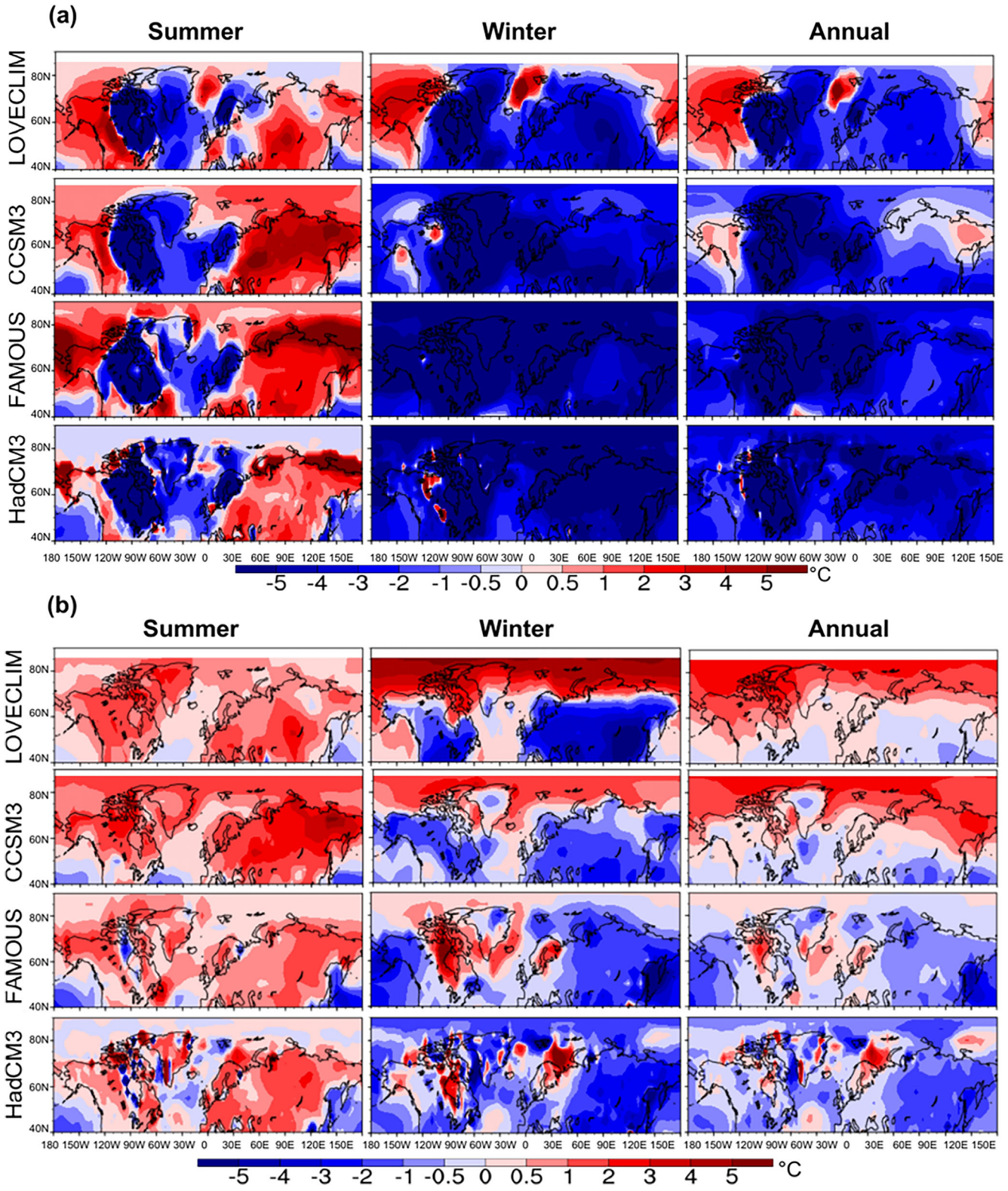

Figure 3. Spatial distribution of simulated temperature anomalies (°C) in the Northern Hemisphere extratropics for the time windows of 11.5 ka (a) and 6 ka (b). The anomalies are relative to 0 ka.

The second group with mismatched temperatures includes Alaska, Arctic and eastern Siberia, as opposite temperature trends (especially in winter) across the models are found.

Temperature over the regions with good inter-model agreement

The simulations show overall good agreements over northern Canada, north-west Europe, north-east Europe, Greenland and central-west Siberia. The ensemble mean temperatures generally rise from the cold initial state until 6–7 ka, followed by a gradual decrease to the levels at 0 ka, with the exception of summer temperature in north-east Europe and central-west Siberia. As indicated by the ensemble mean, the magnitudes of this cool early Holocene vary among regions (Fig. 4). In particular, a considerably cool early Holocene climate is found in northern Canada, with 5 °C lower ensemble mean in summer and

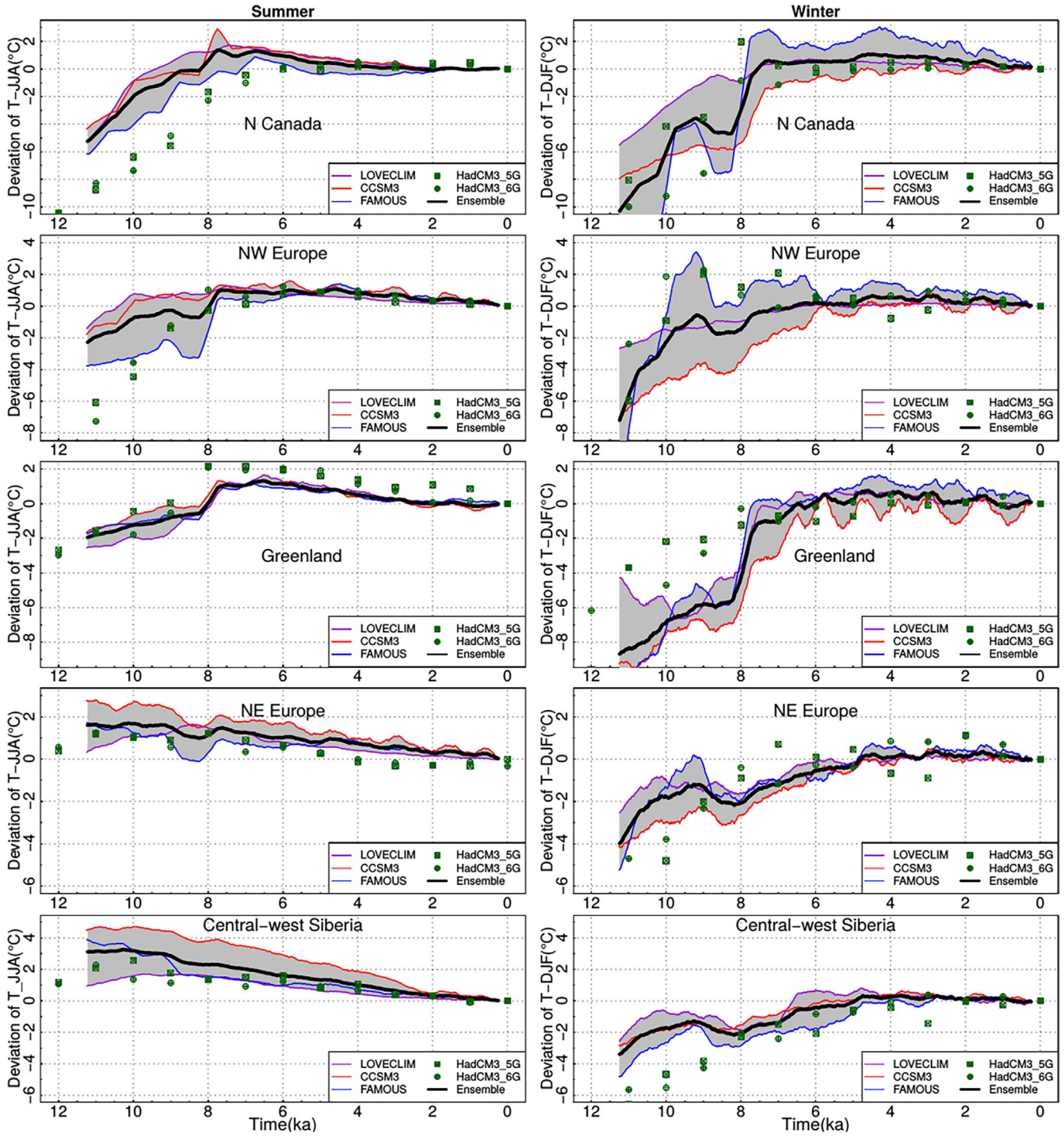

Figure 4. Temperature trends (shown as anomalies from the PI in °C) over the regions where multiple simulations have good agreement, and corresponding multi-model ensemble mean (based on three transient simulations). The grey shading indicates the ensemble range.

10 °C lower in winter, whereas only a minor cooling is present in north-east Europe and central-west Siberia, with about 4 °C cooling in winter and 1–3 °C warming in summer. Temperatures in Greenland and north-west Europe show intermediate values, with a cooling of 2–3 °C in summer and around 8 °C in winter.

Only minor inter-model variations within the range of 3 °C are found in Greenland and north-east Europe during the early Holocene. In Greenland, all simulations indicate about 3 °C cooler summer conditions at 11.5 ka in comparison with 0 ka, followed by a rise to 1 °C at around 7.5 ka. In winter, all simulations suggest low temperatures at 11.5 ka with an approximately −8 °C anomaly of the ensemble mean temperature, notwithstanding the temperature spread between individual simulations of up to 5 °C. In north-east Europe, the simulations suggest a warming of 1 °C in summer and cooling of 4 °C in winter at 11.5 ka, with a 2 °C multi-simulation spread until 9 ka. From 11.5 ka onward, simulated winter temperatures slowly rise to the pre-industrial level, while in summer the temperature anomalies show a gradual decrease of about 1 °C. Over central-west Siberia, temperatures in winter show a 3–4 °C increasing trend during the Holocene, while the simulations indicate 3 °C cooler summers. Within the frame of overall consistent trends, slightly different temperatures are found in northern Canada and north-west Europe during the winter. In northern Canada, the small early Holocene temperature anomalies in LOVECLIM might be related to the use of a fixed modern land–sea mask

throughout the simulation, which implies underestimation of the early Holocene albedo over the Hudson Bay. The jump of simulated winter temperature in FAMOUS at 8 ka might be related to the spike in FWF (Fig. 1). In north-west Europe, the magnitudes of the cooling generally increase in the order of LOVECLIM, CCSM3, HadCM3 and FAMOUS. One exception is that winter temperature anomalies in HadCM3 and FAMOUS rise rapidly to a distinct peak of + 2 °C at around 9–10 ka, leading to high temperatures at about 9 ka. The warm peaks in FAMOUS and HadCM3 are mainly caused by a response of sea ice to the opening of the Bering Strait (Fig. S4). Overall, these roughly consistent patterns demonstrate that over these sub-regions, forced millennial climate change exceeds internal climate variability during the early Holocene.

Temperatures over the regions with less multi-model consistency

In Alaska, Arctic, and eastern Siberia, simulated temperatures show poor consistency (Fig. 5), especially in winter when both positive and negative early Holocene anomalies are simulated by the different models. In Alaska, the spread of simulated winter temperatures at 11.5 ka ranges from 2 °C higher in LOVECLIM to 4–6 °C lower in FAMOUS and HadCM3 in comparison with at 0 ka. This distinct multi-model variation in winter is thus up to 8 °C, which is considerably larger than in summer when the inter-model variation is only 1 °C. Over the Arctic, the discrepancies between the simulations also primarily relate to winter when they are up to 8 °C. At 11.5 ka, the winter temperature anomaly is slightly above 0 °C in LOVECLIM, while more than 8 °C cooling is produced in FAMOUS. Nevertheless, the ensemble mean temperature suggests 1 °C cooling in summer and 4 °C warming in winter throughout the Holocene. Relatively large multi-simulation differences are found over eastern Siberia in both summer and winter, reaching up to 3 °C at the onset of the Holocene. The simulations show decreases in summer temperatures over eastern Siberia throughout the Holocene, with the largest decrease (>4 °C) in CCSM3. This large variation in summer is primarily caused by exceedingly warm early Holocene conditions in CCSM3. In winter, over 2 °C cooling is simulated by LOVECLIM during the Holocene, contrasting with up to 5 °C warming in FAMOUS. The ensemble mean decreases by almost 4 °C in summer, but generally rises by 2 °C in winter despite a small drop at ~8.5 ka.

In general, although the simulations generally agree on temperatures over the large-scale Northern Hemisphere extra-tropics, some regions show better inter-model agreements than others when zoomed to the regional scale. The mismatches among the simulations are large during the early Holocene, and can be outlined as follows: (i) a warm winter climate over Alaska in LOVECLIM in comparison with various degrees of cooling in other models; (ii) large negative temperature deviations (as compared with at 0 ka) over the Arctic in FAMOUS contrasting with slightly positive values in LOVECLIM; and (iii) a stronger summer warming over eastern Siberia in CCSM3 than in other simulations, and a warm winter in LOVECLIM over eastern Siberia contrasting with the cool climate in HadCM3.

Discussion

Comparisons of multi-model simulations provide an opportunity to evaluate the performance of climate models in simulating climate response to radiative forcings and other boundary conditions. The following discussion will start from the above results with a focus on the regions where the simulated temperatures are different, and the causes of these mismatches will be investigated at two levels. We first try to identify the direct causes of these inter-model discrepancies via a diagnosis of various climate variables. The potential origin of these divergent climate variables is then examined.

Divergent climate variables lead to mismatched temperatures

Mismatched Alaskan winter temperature

The relatively warm early Holocene in LOVECLIM results from enhanced southerly winds induced by the Laurentide Ice Sheet (LIS) that bring warm air from the south. These enhanced southerly winds can be identified by examining the anomalous atmospheric circulation over the ice sheets at 11.5 ka, in comparison with the ice-free condition at 0 ka. Atmospheric circulation is indicated in the terms of geopotential height fields, which reflect anomalous geopotential to standard gravity at mean sea level, with high values representing high pressure near the surface. Although there are largely similar responses of geopotential heights to the existence of the LIS, such as enhanced values over the LIS, the magnitude of these anomalies differs across individual models (Fig. 6). At 11.5 ka, winter geopotential heights in LOVECLIM and FAMOUS are up to 50 gpm (geopotential meter) higher over the centre of the LIS than at 0 ka, which is larger than the enhancement of 30 gpm in HadCM3. The LOVECLIM and HadCM3 simulations have similar spatial patterns of Northern Annular Mode with a lower value over the polar region than in the surrounding areas, but with larger anomalies of geopotential height in LOVECLIM than in HadCM3. To further analyse this anomalous geopotential height, the geopotential height differences between the LIS (50–75°N, 65–110°W) and the North Pacific (35–45°N, 120–180°W) were calculated. These results are further standardized to the changes relative to the conditions at 0 ka. This standardized difference of geopotential height in LOVECLIM was up to 70% at 11.5 ka, which declines with time towards 0 ka (Fig. S3). The FAMOUS and HadCM3 simulations also show a similar decreasing trend in geopotential height changes during the Holocene, but with a smaller magnitude than in LOVECLIM. A similarly anomalous atmospheric circulation, with a comparable amplitude of changes as in HadCM3, is indicated by the surface pressure anomaly in CCSM3 (data not shown). Therefore, these different anomalies in geopotential height fields among individual models can lead to divergent climate simulations over the marginal regions of the ice sheet, over which this differential signal is weak and even a minor divergence is visible. In Alaska (to the west of the LIS), the intense warm climate during the early Holocene in LOVECLIM is primarily caused by the strong gradients in geopotential height that induce southerly winds, bringing warm air from the south and increasing the local temperature in Alaska. This effect lasted until the final disappearance of the LIS at 6.8 ka, after which the small decreasing trend in temperature can be linked to a sea ice cooling effect on coastal regions of northern Alaska (Fig. 7). Compared with the HadCM3 simulation, lower temperatures in FAMOUS can be explained by more extended sea ice in this model (Jones *et al.*, 2005), and a stronger anticyclone over Alaska (Fig. 6).

Previous studies have analysed the effect of ice sheets on atmospheric circulation under LGM conditions. The experiment performed by the Polar MM5 atmospheric model has shown that 500-hPa geopotential height over the LIS

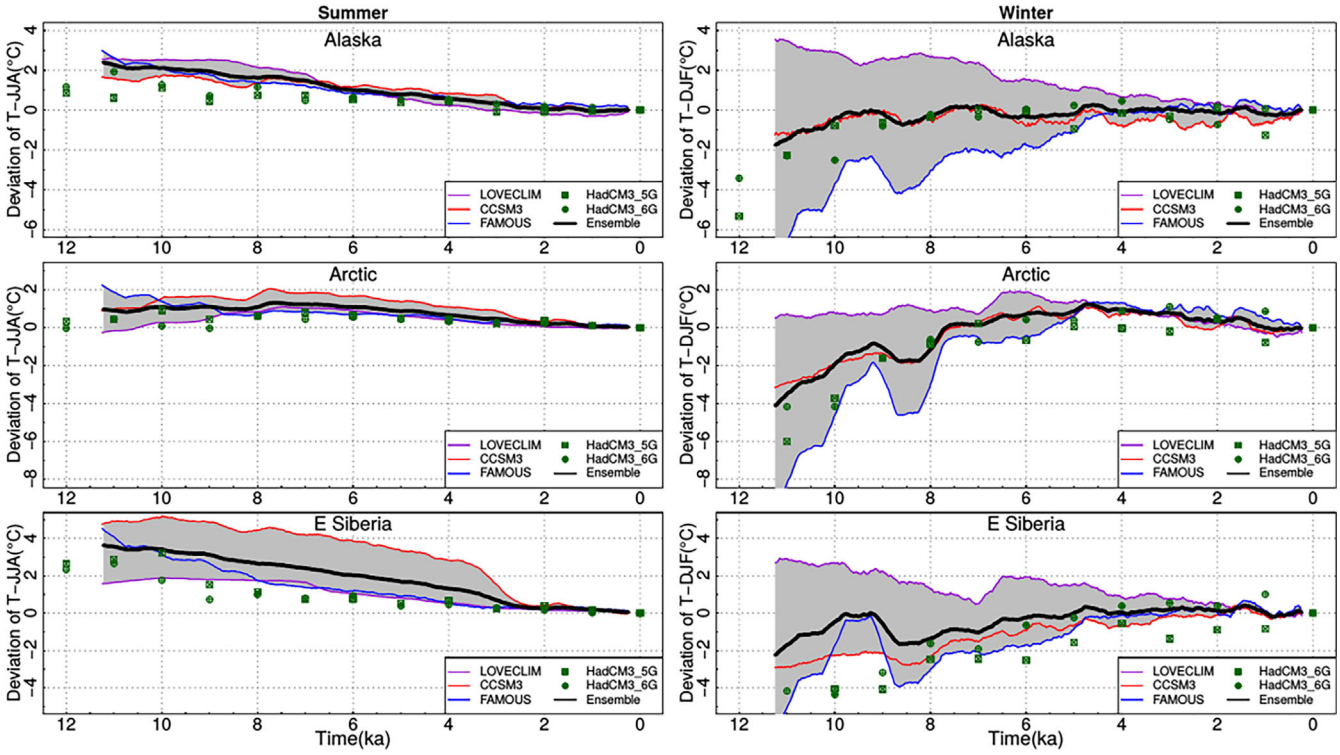

Figure 5. Simulated temperature anomalies (from the PI) over the regions where temperatures are less consistent across the simulations.

increased by 260 gpm in January and 70 gpm in summer (Bromwich *et al.*, 2004, 2005). The intensified atmospheric baroclinicity induced by the ice sheets is suggested as one of the primary mechanisms behind the atmospheric circulation changes under the LGM boundary conditions (Bromwich *et al.*, 2005). Another explanation for these effects is that the airflow can be deflected or split around an anticyclone over the LIS (*e.g.* Bromwich *et al.*, 2004). Sensitivity experiments of the atmospheric circulation response to idealized circular mountains reveal that the orography effects of an ice sheet are highly dependent on the scale of the ice sheet (Yu and Hartmann, 1995). Given the scale of the ice sheets in our experiments, the ice-sheet effects on atmospheric circulation during the early Holocene are much smaller compared with the LGM, as shown in our simulations.

Mismatched winter temperature over Arctic

Over the Arctic, the inter-model divergences of winter temperature during the early Holocene are associated with the different sea ice cover across the individual simulations. Although it is difficult to establish if the sea ice changes are a cause or effect of Arctic temperatures, sea ice plays a critical role in the climate system through sea ice-related feedbacks. First, the areal extent of sea ice determines the extent ot which albedo-related feedback occurs, because the albedo of sea ice is typically up to 0.5–0.6 and significantly higher than for open ocean at high latitudes. Furthermore, the thickness of sea ice influences the amount of heat that is released from the relatively warm ocean to the cold atmosphere (Renssen *et al.*, 2005; Holland *et al.*, 2006). In the four simulations, the early Holocene sea ice anomaly is overall positive compared with at 0 ka (Fig. 7). However, the absolute area of sea ice and the magnitude of anomalous sea ice cover (between 11.5 and 0 ka) varies between the models. At 11.5 ka, the simulated Northern Hemisphere sea ice in March is of the order of 10^{12} m^2 and decreases in the order FAMOUS, CCSM3, HadCM3 and LOVECLIM. The largest change of Northern Hemisphere sea ice in FAMOUS is up to 32×10^{12} m^2, which is twice of the minimum change in HadCM3 and LOVECLIM (Fig. S4). The magnitudes of anomalous sea ice area follow the same order as for absolute sea ice cover, with the largest anomaly in FAMOUS (Fig. S4). It is well known that accurately simulating sea ice in coupled climate models is challenging because of the high complexity of sea ice both spatially and temporally, which can also be seen from the wide spread of simulated sea ice even under pre-industrial conditions. At 0 ka, the Northern Hemisphere sea ice area in these models varies from 13.5×10^{12} to 24×10^{12} m^2 (Fig. S4). Studies have suggested that Northern Hemisphere sea ice was overestimated in CCSM3, FAMOUS and HadCM3 to different degrees and at different spatial patterns (Gordon *et al.*, 2000; Jones *et al.*, 2005; Bryan *et al.*, 2006). For instance, CCSM3 overestimated sea ice in the Labrador Sea, while HadCM3 and FAMOUS simulated more sea ice in the Barents Sea (Gordon *et al.*, 2000; Jones *et al.*, 2005; Bryan *et al.*, 2006). Compared with these total Northern Hemisphere sea ice areas, simulating a consistent anomalous spatial distribution of sea ice is even more difficult, as revealed by various sea ice patterns across these simulations. In particular, thickness anomalies of sea ice over the Greenland Sea in HadCM3 are larger than in LOVECLIM. Therefore, the cooler climate in HadCM3 than in LOVECLIM is partially related to the insulation of thick sea ice in HadCM3 at 11.5 ka. The simulated strong winter cooling at 11.5 ka in FAMOUS could be related to enhanced albedo feedback due to extensive sea ice cover. It is also noticeable that considerable changes of Northern Hemisphere sea ice area in FAMOUS occurred between 9 and 8 ka (Fig. S4), which results from the opening of the Bering Strait and explains why temperature substantially changed around that time. The Atlantic Meridional Overturning Circulation (AMOC) is another associated factor impacting temperatures in the Arctic, especially contributing to climate changes associated with millennial scale events; additional detailed discussion on spatial (Fig. S5) and Holocene trends (Fig. S6) are presented in the Supporting Information.

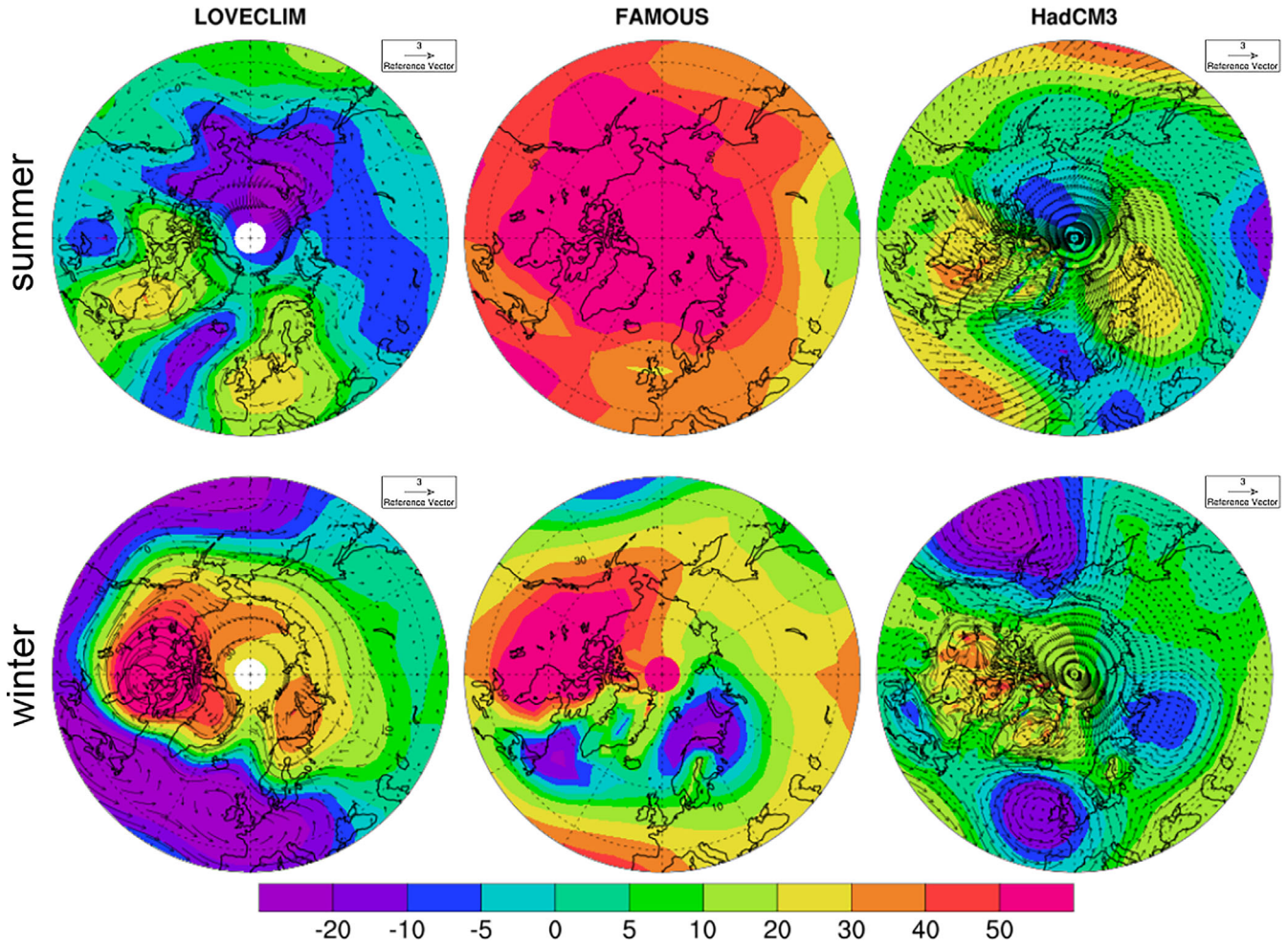

Figure 6. Anomalies in geopotential height fields (11.5–0 ka, in gpm) induced by the ice sheets at 11.5 ka, shown as values at 800 hPa in LOVECLIM, at 850 hPa in FAMOUS and HadCM3. Associated wind anomalies are indicated by the vectors.

A brief comparison with proxy-based sea ice reconstructions broadly supports this simulated extended sea ice extent during the early Holocene. Proxy-based sea ice reconstructions reveal an overall decreased tendency in sea ice extent throughout the Holocene, such as in the circum Arctic areas. The magnitudes of sea ice extension are spatially heterogeneous (de Vernal *et al.*, 2013). In particular, dinocyst assemblages suggest positively anomalous early Holocene sea ice over the regions which were connected to the Atlantic, such as the Labrador Sea and Greenland Sea (de Vernal *et al.*, 2013), which roughly agrees with larger early Holocene sea ice cover in the simulations.

Mismatched temperature in eastern Siberia

As a main contributor to mismatches in multi-simulation temperatures, the intense early Holocene warmth in CCSM3 primarily results from its large negative albedo anomaly (more than −0.2 compared to at 0 ka) in eastern Siberia. Climate is known to be highly sensitive to surface albedo changes (Romanova *et al.*, 2006), and thus inter-model variations in albedo could cause differences in simulated temperatures. The surface albedo anomalies between the early Holocene and the pre-industrial are spatially heterogeneous. On the one hand, the anomalous albedos over the ice sheets are roughly similar. For instance, an enhanced surface albedo of up to 0.6 at 11.5 ka over the LIS is consistently found in all simulations (Fig. 8), despite a small exception over the Hudson Bay in LOVECLIM due to the fixed modern land–sea mask. On the other hand, large inter-model albedo anomalies are found over the regions where surface albedo is primarily influenced by vegetation, snow cover and sea ice cover.

In eastern Siberia, summer surface albedo in CCSM3 differs from other models. In CCSM3, overall Holocene albedo values are higher than 0.36, and they show a rising trend during the Holocene with a rapid increase at 3 ka, whereas other models suggest a stable Holocene trend of summer albedo with absolute values ranging from 0.15 to 0.2 (Fig. S7). This increasing Holocene albedo in CCSM3 is negatively correlated with a decreasing temperature trend, and it is clear that the 2 °C decline at around 3 ka is related to an increase in albedo. This negative anomaly and increased trend of simulated temperature in CCSM3 are due mainly to high albedo at 0 ka, which is up to 0.65. A further investigation of snow cover in the simulation shows that most of eastern Siberia is covered by snow during the summer season, which is clearly an overestimation, as it would imply the inception of a continental ice sheet. By contrast, other simulations show low albedo (around 0.2), indicating a vegetation-covered surface, which is more realistic given the present-day landscape. In winter, the spread of inter-model temperatures over eastern Siberia results from multiple factors. The different albedo response related to snow cover can partly explain the spread across the simulations, with the relatively warm climate in LOVECLIM corresponding to low albedo and the low temperature in FAMOUS associated with high albedo. Moreover, sea ice changes influence the

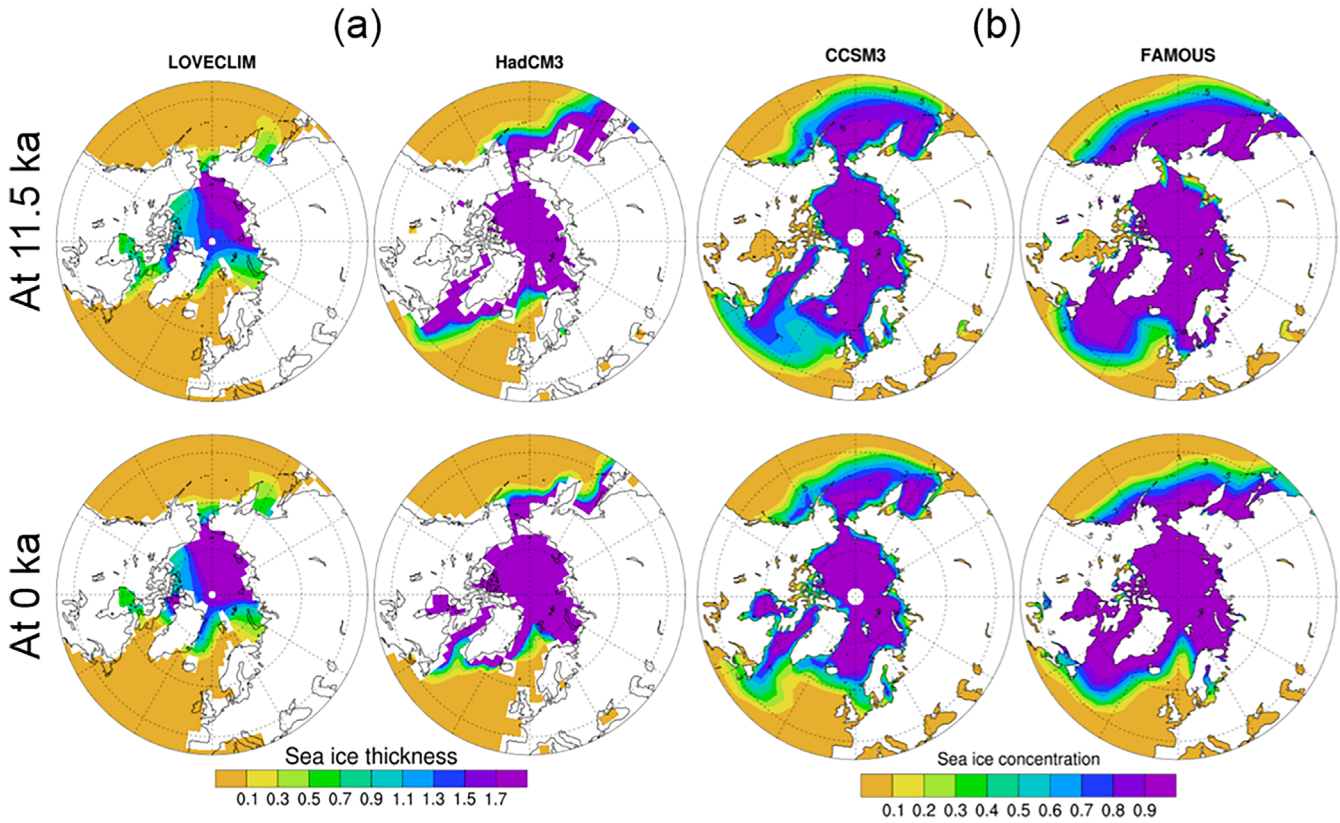

Figure 7. Distribution of maximum sea ice (in Feburary). (a) Ice thickness (m) in LOVECLIM and HadCM3, and (b) sea ice concentration in FAMOUS and CCSM3.

temperature of coastal Siberia. For example, the temperature bump at around 9 ka in FAMOUS and a mild temperature increase in LOVECLIM are caused by temporal variations of sea ice (Fig. S4). Additionally, the warm winter in LOVECLIM is partially associated with the enhanced southerly winds discussed previously.

Potential sources contributing to inter-model divergences of climate variables

Uncertainty of ice-sheet-related forcing

With decaying ice sheets in North America and Fennoscandia, the uncertainty in the FWF forcings during the early Holocene is related mainly to the total volume of ice melt involved, the location of discharge and the timing of discharge, which further impact the Holocene simulations. Different FWF forcing scenarios and associated different AMOC responses have climate impacts through adjustments in heat transport and sea-ice-related feedback (Kageyama *et al.*, 2009; Blaschek and Renssen, 2013). The total amount of FWF can be constrained from both the ocean and the land perspectives, as FWF discharge serves as the link of water exchange between the ocean and continental ice. For instance, the fossil-coral-based estimates of far-field sea level change can reflect the total amount of FWF from the ocean perspective (Lambeck *et al.*, 2014). From the land side, the total amount of FWF can be roughly constrained based on geological indicators of ice-sheet retreat (Peltier, 2004). For the Holocene a total amount of freshwater equivalent to 60 m of sea level was released into the ocean between 11.5 and 6 ka with a large contribution from the LIS (Peltier, 2004; Lambeck *et al.*, 2014). Sensitivity studies have further disclosed that, apart from total amount of FWF, various temporal distributions and geographical locations can induce different responses in ocean circulation (Roche *et al.*, 2010). Although ocean sediment data (*e.g.* detrital carbonate, ice-rafted detritus) and geochemical tracers (*e.g.* $\delta^{18}O$, $^{87}Sr/^{86}Sr$, U/Ca) can provide certain constraints on FWF routing (Carlson *et al.*, 2007; Jennings *et al.*, 2015), it is uncertain how this amount of water was distributed spatially and temporally. First, various magnitudes of FWF are suggested by different proxies. For instance, the geochemical tracer U/Ca suggests a slightly larger FWF discharge for the St. Lawrence River between 12 and 11 ka than indicating by $\delta^{18}O$, probably because additional factors, such as temperature and weathering, modulate the signal of changes in FWF (Carlson *et al.*, 2007). Furthermore, the temporal distributions of FWF in different estimates are not identical. For instance, the curve shapes of these proxy-based FWF estimates differ from the model-based estimates, with the maximum reached at different times (Licciardi *et al.*, 1999; Carlson *et al.*, 2007), which is related to the difficulty in accurately dating samples. Additionally, reaching agreed geographical locations of FWF discharge is hindered by the spatial sparseness of proxy records. Overall, FWF is very uncertain for the early Holocene, especially in terms of discharge rate, location and timing. This uncertainty is also reflected in FWF differences in the four experiments discussed here, which potentially induces some inter-model divergence. To avoid such FWF-related influences, it will be beneficial to construct FWF protocols and apply them in all participating models for a forthcoming inter-comparison project, which would allow us to focus on the dominant climate processes and feedbacks.

Impact of inter-model differences in climate sensitivities

In the present study, climate sensitivities are used to broadly indicate the sensitivity of the climate system to both radiative forcing and FWF forcing. The sensitivity to radiative forcing generally refers to the change in the global annual mean

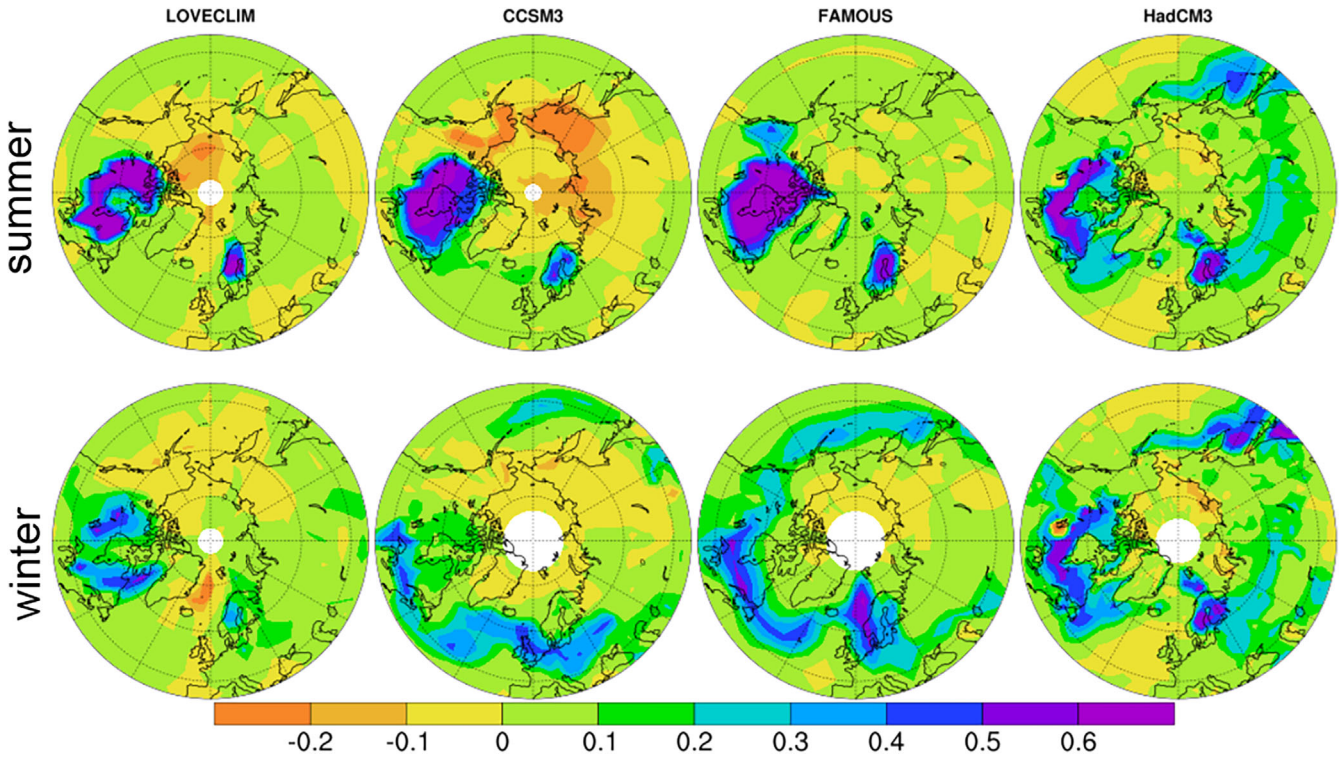

Figure 8. Surface albedo anomalies (shown as fractions) at 11.5 ka compared to at 0 ka.

surface air temperature in response to a doubling of CO_2 (Knutti and Hegerl, 2008), representing a global average. Yet the CSr shows temporal and spatial patterns when examined in detail, as CSr is a function of baseline climate and involves a series of processes on different time scales (Boer and Yu, 2003). In particular, numerous studies have quantitatively examined CSr for decades and have found that it varies for different climate states (Boer and Yu, 2003). CSr generally decreases with a warmer climate and increases with a colder climate (Boer and Yu, 2003; Knutti and Hegerl, 2008). Feedback processes, such as those involving water vapour, lapse rate, surface albedo and clouds, can differ in strength for different climate states (Boer and Yu, 2003; Randall *et al.*, 2007). For simplicity, CSr is assumed to change linearly over small ranges of climate differences, as vital global atmospheric feedbacks remain close to a constant when the threshold value of temperature is not exceeded (Randall *et al.*, 2007). CSr during the early Holocene was reportedly slightly higher than that of 0 ka within this linear assumption, owning to a slightly cooler early Holocene. By contrast, CSr at 6 ka was slightly smaller with a similar linear assumption. However, the exact rate of change of CSr in response to climate states remains of debate. For instance, recent studies suggest weaker CSr enhancements than previously in response to the same amount of cooling (Kutzbach *et al.*, 2013).

CSr varies among individual models, ranging from 2 °C in LOVECLIM to 4 °C in FAMOUS (Table S1). Given this high CSr in FAMOUS and positive radiative forcings during the early Holocene, the climate in FAMOUS would be expected to be warmer than in other simulations when an identical model response to ice sheets is assumed. However, the overall cool climate in FAMOUS seems to conflict with this expectation. A plausible explanation for this paradox is that the expected warmth was overwhelmed by ice-sheet-related cooling. Moreover, the spatial heterogeneity of CSr could outweigh this expected overall warming at certain regions and thus also potentially contributes to this conflict. For instance, Boer and Yu (2003) revealed that the spatial patterns in CSr are due partially to local feedback processes and are reflected by the geographical distribution of the climate sensitivity coefficient. In addition, the FAMOUS results (at 11.5 ka) were obtained from a full transient simulation since the LGM, which implies that the model still had a 'memory' of the preceding cold climates. Further detailed discussions on the spatial pattern of CSr and sensitivity experiments would provide additional information but this is beyond the scope of the present study. The sensitivity of the climate system to freshwater forcing (CSf) varies among these models and associated influences on temperature are discussed in the Supporting Information.

Impacts of the model physics and resolution

Model physics also contribute to inter-model variations. By model physics, we refer to how climatic processes are represented in the model world, without considering external radiative forcings. For instance, in CCSM3, the over-estimated albedo is related to the recently adapted radiative transfer formulation coefficient, which primarily contributes to multi-simulation temperature differences in eastern Siberia. Compared with 0 ka, the early Holocene summer albedo in CCSM3 is reduced by more than 0.2 (Fig. 8), which primarily results from an overestimated albedo at 0 ka (>0.7). Such high albedo can be associated with the later adopted formulation of a radiative transfer coefficient (Collins et al., 2006). According to an assessment of surface albedo (using MODIS data), this new formulation produces extensive snow cover, because white-sky albedo in vegetated areas might be insufficiently simulated and the increase in albedo with solar zenith angle is probably overestimated (Oleson *et al.*, 2003).

The spatial resolution of a model determines the overall level of detail in its representation of climate processes. The detailed representation of key physical processes such as the barrier effect due to topography can improve the accuracy of the simulation. The spatial resolution, however, is limited by

computer power, especially for simulations spanning millennial or longer periods. Lunt *et al*. (2013) found that resolution (effect) could partially explain multi-model differences, such as stronger cooling over the African monsoon region in the General Circulation Model (GCM) than in the Earth System Model of Intermediate Complexity (EMIC), but also stated that this should be confirmed with further analysis. Some resolution-related patterns are observed when the atmosphere and ocean components are individually examined. For instance, the widely extended sea ice in FAMOUS is mainly caused by a relatively coarse spatial resolution in the ocean component (Gordon *et al*., 2000; Jones *et al*., 2005). Although FAMOUS has similar physical and dynamic processes to HadCM3, this coarse resolution may lead to insufficient heat transport, such as in the Barents Sea, which ultimately leads to overestimated sea ice cover in that region (Gordon *et al*., 2000; Jones *et al*., 2005). This overestimated sea ice cover can cause cool Arctic climate through an enhanced albedo feedback (Renssen *et al*., 2005). In addition, the intense Alaskan warmth in winter in LOVECLIM might be related to its coarse vertical resolution, implying a relatively poor representation of the LIS topography. Therefore, resolution improvement would be a major factor when this improvement is related to improved representation of dynamic processes. Nevertheless, to further investigate these resolution-related effects, more analyses, such as using proxy data to evaluate the simulated early Holocene climate and applying a fully identical set-up procedure, are needed.

Conclusions

Transient features of the early Holocene climate potentially introduce large uncertainties in simulating Holocene temperatures. To narrow these uncertainties and analyze the temperature trends, we compared four Holocene simulations performed with different models. The main findings are outlined as follows:

1. Consistently simulated Holocene temperatures in multi-model simulations

   Over the large scale of the Northern Hemisphere extratropics, the simulated temperatures are generally consistent among models with better agreements in summer than in winter, which is characterized by an early Holocene warming, mid-Holocene maximum and gradual decrease towards 0 ka. On a regional scale, reasonably consistent temperature trends are found where climate is strongly influenced by the ice sheets, including Greenland, northern Canada, northern Europe and central-west Siberia. These simulated temperatures generally follow a similar pattern to that noted above. Within these general patterns, the magnitude of early Holocene warming slightly varies with regions. The strongest early Holocene warming, up to 5 °C in summer and 10 °C in winter, is found in northern Canada, whereas north-east Europe and central-west Siberia show the least warming magnitude, with 4 °C warming in winter and 1–3 °C cooling in summer. An intermediate degree of warming is found in Greenland and north-west Europe, with about 2 °C in summer and 8 °C in winter. Overall, these generally consistent temperature trends illustrate that forced climate change overwhelms the structural and parametric uncertainties, implying that the temperature trends are relatively well established in these regions.
2. Differences of the multi-model simulations and their direct causes

   Large inter-model variations exist in Alaska, the Arctic and eastern Siberia. In particular, the signals of individual model simulations are incompatible during the early Holocene. On the one hand, the strong southerly winds induced by the LIS over Alaska and part of eastern Siberia result in an anomalous warm climate in LOVECLIM. Higher summer temperatures (1–2 °C) over eastern Siberia in CCSM3 than in other models are caused by a strongly negative albedo anomaly between 11.5 and 0 ka, which ultimately is associated with a high albedo at 0 ka. On the other hand, the wide spread of simulated winter temperatures over the Arctic can be partially attributed to cold climate in FAMOUS due to its extensive sea ice cover. This extended early Holocene sea ice cover influences the strength of the albedo-related feedback and could explain why winter temperature in FAMOUS is 2–3 °C lower than the ensemble mean.
3. Possible sources contributing to the different responses of climate variables

   The multi-model comparisons reveal that varied responses in the models can be caused by the model physics, model resolution and model-dependent sensitivities. For instance, the later adopted radiative transfer formulations in CCSM3 may cause an overestimated albedo over Siberia at 0 ka. Moreover, relatively simplified sea ice representation in FAMOUS may lead to overestimated sea ice cover. Also, the coarse vertical resolution in LOVECLIM might result in overestimated responses of atmospheric circulation to the LIS over Alaska. This inter-model comparison is partially hampered by the differences between the experimental set-ups and forcings, especially concerning FWF, which has a major impact on the early Holocene climate. Hence, using a standardized FWF for the early Holocene would be advantageous for future inter-model comparisons.

Supporting Information

1. Models and climate forcings
2. Discussion on AMOC, including Simulated AMOC and impact of inter-model differences in climate sensitivities

Table S1. Summary of the climate models investigated.

Figure S1. Orbital-scale insolation and GHG-related radiative forcing during the Holocene.

Figure S2. Eight selected regions are marked as boxes. The background colour indicates the simulated annual mean temperature in LOVECLIM at 11.5 ka.

Figure S3. Atmospheric circulation changes induced by the topography of the LIS, shown as differences in geopotential height between the LIS and North Pacific. Given different vertical layers among the models, the results are standardized by calculating the anomalies and percentage with regard to the 0 ka condition. The results are shown as 100-year average in LOVECLIM and 1-ka interval in FAMOUS and HadCM3.

Figure S4. Total area of sea ice in the Northern Hemisphere ($\times 10^{12}$ m^2).

Figure S5. Meridional overturning streamfunction (in Sv) of the Atlantic Basin in the transient simulations.

Figure S6. Changes of maximum AMOC (in the box of 500–2000 m, 34°S–50°N, according to the definition of Hofer *et al*, 2011; Drijfhout *et al*, 2012) over the course of the Holocene. Results are shown as 100-yr averages.

Figure S7. Albedo changes over the course of the Holocene.

Acknowledgements. The China Scholarship Council and Academy of Finland (EBOR project) are acknowledged for their financial support. We would like to thank two anonymous reviewers and the Editor for their constructive comments.

Abbreviations. AMOC, Atlantic Meridional Overturning Circulation; CSr, climate sensitivity to radiative forcings; FWF, freshwater flux; GHG, greenhouse gases; ISC, ice-sheet configuration; LGM, Last Glacial Maximum; LIS, Laurentide Ice Sheet; ORB, orbital forcing

References

Bakker P, Masson-Delmotte V, Martrat B *et al.* 2014. Temperature trends during the present and last interglacial periods – a multi-model-data comparison. *Quaternary Science Reviews* **99**: 224–243.

Blaschek M, Renssen H. 2013. The Holocene thermal maximum in the Nordic Seas: the impact of Greenland Ice Sheet melt and other forcings in a coupled atmosphere-sea ice-ocean model. *Climate of the Past* **9**: 1629–1643.

Boer GJ, Yu B. 2003. Climate sensitivity and climate state. *Climate Dynamics* **21**: 167–176.

Braconnot P, Joussaume S, de Noblet N *et al.* 2000. Mid-Holocene and Last Glacial Maximum African monsoon changes as simulated within the Paleoclimate Modelling Inter-comparison Project. *Global and Planetary Change* **26**: 51–66.

Brewer S, Guiot J, Torre F. 2007. Mid-Holocene climate change in Europe: a data-model comparison. *Climate of the Past* **3**: 499–512.

Bromwich DH, Toracinta ER, Oglesby RJ *et al.* 2005. LGM summer climate on the southern margin of the Laurentide ice sheet: wet or dry? *Journal of Climate* **18**: 3317–3338.

Bromwich DH, Toracinta ER, Wei H *et al.* 2004. Polar MM5 simulations of the winter climate of the Laurentide Ice Sheet at the LGM. *Journal of Climate* **17**: 3415–3433.

Bryan FO, Danabasoglu G, Nakashiki N *et al.* 2006. Response of the North Atlantic Thermohaline circulation and ventilation to increasing carbon dioxide in CCSM3. *Journal of Climate* **19**: 2382–2397.

CAPE project members. 2001. Holocene paleoclimate data from the arctic: Testing models of global climate change. *Quaternary Science Reviews* **20**: 1275–1287.

Carlson AE, Clark PU, Haley BA *et al.* 2007. Geochemical proxies of North American freshwater routing during the Younger Dryas cold event. *Proceedings of the National Academy of Sciences of the United States of America* **104**: 6556–6561.

Collins WD, Bitz CM, Blackmon ML *et al.* 2006. The community climate system model Version 3 (CCSM3). *Journal of Climate* **19**: 2122–2143.

de Vernal A, Hillaire-Marcel C, Rochon A *et al.* 2013. Dinocyst-based reconstructions of sea ice cover concentration during the Holocene in the Arctic Ocean, the northern North Atlantic Ocean and its adjacent seas. *Quaternary Science Reviews* **79**: 111–121.

Dyke AS, Moore A, Robertson L. 2003. Deglaciation of North America, *Open-File Report-Geological Survey of Canada*.

Drijfhout S, van Oldenborgh GJ, Cimatoribus A. 2012. Is a decline of AMOC causing the warming hole above the North Atlantic in observed and modeled warming patterns? *Journal of Climate* **25**: 8373–8379.

Flato G *et al.* editors. 2013. Evaluation of climate models. In: *Climate Change 2013: the Physical Science Basis. Contribution of Working Group I to the Fifth Assessment Report of the Intergovernmental Panel on Climate Change*, Stocker TF *et al.* (eds). Cambridge University Press: Cambridge.

Gordon C, Cooper C, Senior CA *et al.* 2000. The simulation of SST, sea ice extents and ocean heat transports in a version of the Hadley Centre coupled model without flux adjustments. *Climate Dynamics* **16**: 147–168.

Harrison SP, Jolly D, Laarif F *et al.* 1998. Intercomparison of simulated global vegetation distributions in response to 6 kyr BP orbital forcing. *Journal of Climate* **11**: 2721–2742.

He F. 2011. *Simulating transient climate evolution of the last deglaciation with CCSM3*. Dissertation, University of Wisconsin-Madison.

Hofer D, Raible CC, Stocker TF. 2011. Variations of the Atlantic meridional overturning circulation in control and transient simulations of the last millennium. *Climate of the Past* **7**: 133–150.

Holland MM, Bitz CM, Hunke EC *et al.* 2006. Influence of the sea ice thickness distribution on polar climate in CCSM3. *Journal of Climate* **19**: 2398–2414.

Jennings A, Andrews J, Pearce C *et al.* 2015. Detrital carbonate peaks on the Labrador Shelf, a 13-7ka template for freshwater forcing from the Hudson Strait outlet of the Laurentide Ice Sheet into the subpolar gyre. *Quaternary Science Reviews* **107**: 62–80.

Jiang D, Lang X, Tian Z *et al.* 2012. Considerable model-data mismatch in temperature over China during the mid-Holocene: results of PMIP simulations. *Journal of Climate* **25**: 4135–4153.

Jones CD, Gregory JM, Thorpe RB *et al.* 2005. Systematic optimisation and climate simulation of FAMOUS, a fast version of HadCM3. *Climate Dynamics* **25**: 189–204.

Kageyama M, Mignot J, Swingedouw D *et al.* Marzin C. 2009. Glacial climate sensitivity to different states of the Atlantic Meridional Overturning Circulation: results from the IPSL model. 2009. Glacial climate sensitivity to different states of the Atlantic meridional overturning circulation: results from the IPSL model. *Climate of the Past* **5**: 551–570.

Liu Z, Zhu J, Rosenthal Y, *et al.* 2014. The Holocene temperature conundrum. *Proceedings of the National Academy of Sciences USA* **111**: E3501–3505.

Knutti R, Hegerl GC. 2008. The equilibrium sensitivity of the earth's temperature to radiation changes. *Nature Geoscience* **1**: 735–743.

Kutzbach JE, He F, Vavrus SJ *et al.* 2013. The dependence of equilibrium climate sensitivity on climate state: applications to studies of climates colder than present. *Geophysical Research Letters* **40**: 3721–3726.

Lambeck K, Rouby H, Purcell A *et al.* 2014. Sea level and global ice volumes from the Last Glacial Maximum to the Holocene. *Proceedings of the National Academy of Sciences USA* **111**: 15296–15303.

Licciardi JM, Teller JT, Clark PU. 1999. Freshwater routing by the Laurentide Ice Sheet during the last deglaciation, mechanism of global climate change at millennial time scales. *Geophysical Monograph* **112**: 177–201.

Lohmann G, Pfeiffer M, Laepple T *et al.* 2013. A model-data comparison of the Holocene global sea surface temperature evolution. *Climate of the Past* **9**: 1807–1839.

Lunt DJ, Abe-Ouchi A, Bakker P *et al.* 2013. A multi-model assessment of last interglacial temperatures. *Climate of the Past* **9**: 699–717.

Marcott SA, Shakun JD, Clark PU *et al.* 2013. A reconstruction of regional and global temperature for the past 11, 300 years. *Science* **339**: 1198–1201.

Oleson KW, Bonan GB, Schaaf C *et al.* 2003. Assessment of global climate model land surface albedo using MODIS data. *Geophysical Research Letters* **30**: 1143.

Peltier WR. 2004. HIobal glacial isostasy and the surface of the Ice-Age Earth: the ICE-5G (VM2) model and GRACE. *Annual Review of Earth and Planetary Sciences* **32**: 111–149.

Randall DA, Wood RA *et al.* 2007. Cilmate models and their evaluation. In *Climate Change 2007: the Physical Science Basis. Contribution of Working Group I to the Fourth Assessment Report of the Intergovernmental Panel on Climate Change*, Solomon S, Qin D, Manning M, *et al.* (eds). Cambridge University Press: Cambridge; 589–662.

Renssen H, Goosse H, Fichefet T *et al.* 2005. Simulating the Holocene climate evolution at northern high latitudes using a coupled atmosphere-sea ice-ocean-vegetation model. *Climate Dynamics* **24**: 23–43.

Roche DM, Wiersma AP, Renssen H. 2010. A systematic study of the impact of freshwater pulses with respect to different geographical locations. *Climate Dynamics* **34**: 997–1013.

Romanova V, Lohmann G, Grosfeld K. 2006. Effect of land albedo, CO_2, orography, and oceanic heat transport on extreme climates. *Climate of the Past* **2**: 31–42.

Shakun JD, Clark PU, He F *et al*. 2012. Global warming preceded by increasing carbon dioxide concentrations during the last deglaciation. *Nature* **484**: 49–54.

Singarayer JS, Valdes PJ. 2010. High-latitude climate sensitivity to ice-sheet forcing over the last 120 kyr. *Quaternary Science Reviews* **29**: 43–55.

Yu JY, Hartmann DL. 1995. Orographic influences on the distribution and generation of atmospheric variability in a GCM. *Journal of the Atmospheric Sciences* **52**: 2428–2443.

Zhang Y, Renssen H, Seppä H. 2016. Effects of melting ice sheets and orbital forcing on the early Holocene warming in the extratropical Northern Hemisphere. *Climate of the Past* **12**: 1119–1135.